Aerospace Science and Technology 13 (2009) 466–474

Contents lists available at ScienceDirect

Aerospace Science and Technology

www.elsevier.com/locate/aescte

Simulation of unsteady combustion in a LOX-GH_2 fueled rocket engine

M. Masquelet [a], S. Menon [a,*], Y. Jin [b], R. Friedrich [b]

[a] School of Aerospace Engineering, Georgia Institute of Technology, Atlanta, USA
[b] Technishe Universität München, München, Germany

ARTICLE INFO

Article history:
Received 24 May 2008
Received in revised form 11 July 2009
Accepted 27 July 2009
Available online 29 July 2009

Keywords:
CFD
LES
Gaseous hydrogen
Liquid oxygen
Rocket engine
Combustion

ABSTRACT

This paper presents results from an investigation of unsteady combustion inside a small-scale, multi-injector liquid rocket engine. A time-accurate approach in an axisymmetric geometry is employed to capture the unsteady flow features, as well as the unsteady heat transfer to the walls of the combustion chamber. Both thermally perfect gas (TPG) and real gas (RG) formulations are evaluated for this LOX-GH_2 system. The Peng–Robinson cubic equation of state (EoS) is used to account for real gas effects associated with the injection of oxygen. Realistic transport properties are computed but simplified chemistry is used in order to achieve a reasonable turnaround time. Results show the importance of the unsteady dynamics of the flow, especially the interaction between the different injectors. The RG EoS, despite a limited zone of influence, is shown to govern the overall chamber behavior. The sensitivity of the results to changes in the system parameters is studied and some general trends are discussed. Although several features of the simulations agree well with past experimental observations, prediction of heat flux using a simplified flux boundary condition is not completely satisfactory. Reasons for this discrepancy are discussed in the context of the current axisymmetric approach.

1. Introduction

Modeling combustion inside a modern liquid-fueled rocket engine presents a variety of difficult challenges. It involves very high pressures, as well as a wide range of temperatures, from the cryogenic injection temperature (as low as 100 K) to the very high flame temperature (about 3600 K in a real engine) of the liquid oxygen-gaseous hydrogen (LOX-GH_2) system. Thus, real gas effects may be significant, especially the trans-critical event (transition from liquid to supercritical fluid) during LOX injection. The wide range of thermo-physical properties of the species of interest also adds to the complexity of real gas flows. The current effort is focused on developing a self-consistent methodology that can be used to simulate high-pressure combustion in realistic rocket engines. An eventual goal of this effort is to predict unsteady dynamics in such devices and their impact on the heat flux to the combustion chamber walls. This predictive capability could be very useful as these complex flows are nearly impossible to interrogate experimentally.

Time accurate studies of rocket engine combustion are only recently becoming feasible due to the advent of massively parallel computers. In the past, steady state studies [4] have been the norm but recently unsteady simulations have included axisymmetric Large Eddy Simulations (LES) of supercritical mixing [37] and rocket engine studies of single injector configurations [14,22]. In these latter studies, the limited size of the domain of interest allowed simulation of LOX injection under sub-critical conditions for which a very high resolution was required due to the large density gradients. Thus, the three-dimensional computational domain used by Oefelein [22] needed around 12 million grid points for a single, small-scale injector, a prohibitive requirement for parametric analysis.

Past studies do provide some conclusions worth highlighting. The anchoring of the flame to the LOX post tip was first observed experimentally by Mayer et al. [17,18] and later confirmed by another set of experiments summarized by Candel et al. [2] and Habiballah et al. [11]. This result was reproduced numerically by Oefelein [23] with the use of the Peng–Robinson real gas equation of state (PR-EoS) and truly sub-critical injection. Thus, the PR-EoS appears to be an acceptable EoS for real gas studies, and is the one chosen here. More uncertainty exists for the real gas modeling of transport properties. Some recent DNS studies of non-reacting temporal mixing layers of real gases [12,15] have reported that Soret and Dufour cross-diffusion effects are important. However, Oefelein [23] finds only a small influence of these effects on minor species in a reacting flow study. Since modeling of these terms for LES studies remains to be properly developed and validated [26,33], they will be neglected in the present study. Finally, other studies [36] on supercritical mixing or considering other fuel/oxidizer combinations than H_2/O_2 could bring further insight on the phys-

* Corresponding author at: Computational Combustion Laboratory, School of Aerospace Engineering, 270 Ferst Drive, Atlanta, GA 30332-0150, USA. Tel.: +1 404 894 1409; fax: +1 404 894 2760.
E-mail address: suresh.menon@ae.gatech.edu (S. Menon).

1270-9638/$ – see front matter
doi:10.1016/j.ast.2009.07.005

ical processes at stake but are not directly relevant to the current study.

The actual configuration of a typical rocket engine of current interest is complex and three-dimensional. The center of interest of this study is a caloric, water-cooled, sub-scale chamber developed by the German Space Agency in order to investigate the heat flux evolution in a cryogenic LOX-GH_2 combustion chamber at high pressures. The injector plate consists in 19 coaxial injection elements and a full 3D LES with real gas modeling of such a configuration would be computationally very expensive. Therefore, assumptions are made here to limit computational cost and their implications on mixing and combustion processes are discussed in this paper.

2. Formulation

2.1. Governing equations

In order to maintain computational tractability, we restrict our simulations to an axisymmetric configuration, which implies many restrictions since the injector plate with its 19 injection elements is not axisymmetric. This injector plate is modeled as made of concentric injector slots, whose dimensions are such that flow conditions representative of the real engine, and in particular the mass flow rates, can be maintained. A major restriction of the axisymmetric assumption is that flow motion across the centerline is not allowed and radial turbulent diffusion is very limited along the centerline, resulting in a very different behavior from the full 3D case. For the conditions simulated here, these restrictions may not be of great importance since the centerline injector only represents 1/19 of the flow rate. It is important to note that a partial 3D simulation, modeling only a sector of the combustion chamber, would suffer from the same limitation [32].

Following earlier work on real gas combustion LES modeling in a rocket engine [24], we simulate the compressible, unsteady axisymmetric equations using an LES formulation. It is well understood that a true LES would require a full 3D simulation but this approach seems justified here for four major reasons: (a) the prohibitive computational cost of full 3D LES of a multi-injector configuration, (b) the many unknowns in the sub-grid closure that remain to be resolved before full 3D LES can be attempted, (c) a fine resolution can be used in an axisymmetric approach, thereby resolving all important scales of motion at a moderate computational cost, and (d) in the axisymmetric LES approach (as opposed to steady state methods) the modeled dissipation scales with the local grid size through the eddy viscosity. In spite of the limitation of the axisymmetric approach, we believe it contains sufficient physics of mixing and combustion to be useful for study of multi-injector rocket engines. Other axisymmetric unsteady simulations have been reported earlier, with [35,38] or without [3] turbulence modeling.

The axisymmetric LES equations are obtained by Favre spatial filtering [8] and solve the continuity, axial momentum, radial momentum, total energy and species equations. They include an axisymmetric source term similar to a viscous stress and their details can be found elsewhere [16]. Specifically, the heat flux vector is written in its "Irving–Kirkwood" form, that is including the enthalpy flux by mass diffusion, and the diffusion velocities are approximated using Fickian diffusion (as noted earlier, Soret and Dufour terms are neglected). The pressure is determined from the filtered EoS. Using a general form $p = Z\rho RT$, which defines the compressibility factor Z, we obtain:

$$\overline{p} = \overline{\rho} R_u \sum_{k=1}^{n} \left(\frac{\tilde{Z}\tilde{Y}_k\tilde{T}}{W_k} \right) + \overline{\rho} R_u \sum_{k=1}^{n} \left(\frac{\overline{ZYT} - \tilde{Z}\tilde{Y}_k\tilde{T}}{W_k} \right) \tag{1}$$

Here, R_u is the universal gas constant and W_k is the molecular weight for the k-th species. The first term on the right-hand side contains only resolved variables: $\tilde{Z}, \tilde{Y}_k, \tilde{T}$. The second term includes a triple correlation of the temperature, compressibility and species terms and is a term that requires closure. For thermally perfect gases, the filtered EoS is the same as Eq. (1) except that $Z = 1$. It has been shown [9] that the sub-grid term in the above equation is negligible for low heat release in a perfect gas, and it seems to be also the case for real gases [33] even though this has not been clearly demonstrated for a reacting case as yet.

For the closure of the governing equations, a transport equation for the sub-grid kinetic energy k^{sgs} is solved and sub-grid terms are either neglected or modeled using simple gradient diffusion approaches and local eddy viscosity. Further discussion of these sub-grid terms can be found elsewhere [16]. The first concern of this study is to demonstrate the feasibility of this unsteady approach in rocket engine applications and thus the robustness of the closure approach was the priority. Parametric studies on the two model parameters C_ν and C_ε showed very little influence on the results with the current grid, demonstrating that most of the important scales were being resolved, especially in the injector region of high shear mixing. Additional work will be required on more elementary problems to assess the accuracy of various closure models for this specific application, such as the localized dynamic procedure used to compute the closure model coefficients or the linear eddy mixing [31], used to provide advanced closure to the species equation, especially with chemical reactions.

2.2. Real gas equation of state

In a liquid rocket engine operating at high pressures, while the hydrogen still behaves mostly like an ideal gas, the oxygen will behave very differently under supercritical conditions. Therefore, this effect needs to be modeled by using a Real Gas Equation of State (RG EoS). Several equations of state have been developed to describe the behavior of a supercritical fluid. It has been noted [6,24] that the cubic Peng–Robinson equation of state (PR-EoS) is a good choice from accuracy and cost considerations, capable of handling sub-critical injection if required and reducing smoothly to the ideal gas behavior when conditions dictate it in the burned gases. In the current study, we employ this EoS with inflow conditions such that oxygen is injected at supercritical conditions. The general PR-EoS is written as:

$$p = \frac{R_u T}{V - B_m} - \frac{A_m}{V^2 + 2VB_m - B_m^2} \tag{2}$$

with p in bar, $R_u = 83.1447\ \mathrm{bar\,cm^3\,mol^{-1}\,K^{-1}}$, T in K, V in $\mathrm{cm^3\,mol^{-1}}$, A_m in $\mathrm{bar\,(cm^3\,mol^{-1})^2}$ and B_m in $\mathrm{cm^3\,mol^{-1}}$. The mixture parameters A_m and B_m are computed from the pure species properties [20,29] using the corresponding state principle and classical van der Waals mixing laws. A detailed formulation can be found elsewhere [19]. All the terms in the mixture parameters are computed once and for all at the beginning of a simulation except for the temperature dependent term in the A_m term:

$$\alpha(T_{r(ij)}) = \left[1 + f(\Omega_{ij})\left(1 - \sqrt{T_{r(ij)}}\right)\right]^2 \tag{3}$$

$$f(\Omega_{ij}) = 0.37964 + 1.4850\Omega_{ij} - 0.16442\Omega_{ij}^2 + 0.01666\Omega_{ij}^3 \tag{4}$$

This expression for $f(\Omega_{ij})$ is based on modifications made to the initial formulation and validated by Tsonopoulos [34].

Details of the computation of the thermodynamic and transport properties, as well as the iterative process performed in the main solver to compute temperature and pressure from density and energy are not detailed here, for brevity. The transport properties are computed using the methodology developed by Chung

et al. [5], which is considered most effective in terms of computational cost and accuracy [6]. The iterative process is similar to the one described by Okong'o et al. [27]. It should be noted that both procedures are independent and thus it is possible, as demonstrated later, to run any thermodynamic model such as Calorically Perfect Gas (CPG), Thermally Perfect Gas (TPG) or Real Gas (RG) with any transport properties framework such as the multi-species Sutherland's law model used for perfect gas computations or the Chung's model.

2.3. Chemistry

Considering the uncertainty of the turbulent combustion closure model and the need for a relatively quick computational turnaround, simplified reaction mechanisms were used in the current study. An infinite-rate, one-step reduced mechanism [30], suggested by Astrium Corporation, is used for the simulations reported in the first part of the results section, while a finite-rate two-step mechanism [7] is used for the final comparison between TPG and RG simulations. For both mechanisms, a modified version of the sub-grid Eddy Break-Up (EBU) model is used to bound the chemical rates with a mixing rate dependent on the dissipation rate of turbulent eddies which mix reactants at the smallest scales. The formulation for multi-step, finite-rate chemistry is given by Brink et al. [1]. In addition, a lower, non-zero bound is adopted for the mixing rate so that there is some reaction in regions where the sub-grid kinetic energy approaches zero. While the validity of the EBU approach in the current application is difficult to assess, sensitivity of predictions to the value of the model parameter C_{EBU} was found to be minimal for values of the order of the nominal value of unity.

2.4. Boundary conditions

Boundary conditions are very important in numerical simulations and have to be implemented with great care. The current engine configuration uses a choked nozzle at the exit, so outflow is supersonic and requires no additional information to compute the properties inside the computational domain. During the choking process, a backpressure of 1 atmosphere, representative of experimental conditions, is applied until the flow in the nozzle is fully supersonic. At the inflow, the mass flow rate, the temperature and the mixture composition are fixed while the density and axial velocity vary with the pressure. Characteristic based inflow boundary conditions for real gas are then used, following Okong'o et al. [25]. These parameters are given in Table 2 for the simulations of interest in this paper. Because of grid requirements and lack of experimental data, flat velocity profiles are applied as upstream boundary conditions and are allowed to evolve until the injection plane.

The isothermal wall boundary condition for temperature is critical for the wall heat flux prediction. A second-order accurate approach has been implemented, with the temperature at the interface between the flow cell and the ghost cell remaining constant through time. In reality, the gas-side wall temperature is probably not constant in time. The actual engine employed external cooling jackets around the combustion chamber. Thus only the steady state temperature on the coolant side is measured and the exact wall temperature on the inside wall of the engine is not known. Future studies could look into a coupled flow and wall solver, where the transport of heat in the walls would be solved and where the external coolant temperature would be used as boundary condition.

3. Numerical implementation

The governing equations are solved using a finite volume, predictor–corrector scheme, that is second-order accurate in time and fourth-order accurate in space. To suppress initial transients explicit artificial dissipation is included using a combined second-fourth-order dissipation scheme. The RG EoS involves many complex operations such as real-powers, square roots, logarithms, etc. More than 20% of the CPU time is used for these operations. The computation of the transport properties also requires similar operations. Analysis showed that these transport properties vary slowly with time and in the current study, were computed every third time step to reduce computational cost. The overall error introduced is estimated to be less than 0.1%.

Table 1
Physical and computational dimensions of the modified outer injectors.

Entry O_2 radius (Exp.)	2.15 mm
Entry O_2 radius (2D-axi)	1.129 mm
Entry O_2 grid points (2D-axi)	16
Exit O_2 radius (Exp.)	3.15 mm
Exit O_2 radius (2D-axi)	1.8604 mm
Exit O_2 grid points (2D-axi)	16
Tip wall width (Exp.)	0.325 mm
Tip wall width (2D-axi)	0.325 mm
Tip wall grid points (2D-axi)	6
Lower H_2 width (Exp.)	0.475 mm
Lower H_2 width (2D-axi)	$\approx$ 0.444 mm
Lower H_2 grid points (2D-axi)	7
Upper H_2 width (Exp.)	0.475 mm
Upper H_2 width (2D-axi)	$\approx$ 0.386 mm
Upper H_2 grid points (2D-axi)	6

Table 2
Physical conditions at the inflow of the combustion chamber.

	Exp.	TPG Sim.	RG Sim.
Pressure	100 bar	100 bar	100 bar
Mixture ratio	5.964	5.964	5.964
O_2 velocity	11 m s^{-1}	66 m s^{-1}	41 m s^{-1}
O_2 temperature	101.3 K	201.3 K	201.3 K
H_2 velocity	270 m s^{-1}	150 m s^{-1}	164 m s^{-1}
H_2 temperature	106.4 K	106.4 K	106.4 K
Total flow rate	8.81 kg s^{-1}	8.81 kg s^{-1}	8.81 kg s^{-1}

Table 1 gives the precise dimensions for the outer injectors as well as some information on the Cartesian structured grid with the highest resolution. The tip walls between the oxygen and hydrogen channels are resolved with only a few points, as are the hydrogen channels. Due to the small dimensions (less than half a millimeter) of these channels, this resolution still leads to a radial spacing of the order of 50 microns. Near the engine sidewall, where the wall heat flux is measured, a wall-normal grid spacing of 20 microns is used. For comparison, using time-averaged results from the current simulations, Kolmogorov scales in the near-field can be roughly estimated to a few microns, which seem to indicate a reasonable resolution of the energy-containing scales. The grid in the vicinity of the injection plane is nearly uniform with an aspect ratio close to 1 and is slowly stretched in the axial direction as we move downstream. The maximum grid stretching is 5% axially and 7% radially. Grid resolution issues were investigated primarily to ensure that all the features near the injector lips were well resolved. Based on these studies we employ a grid of 601×382 in (x, y) directions for all the reported RG simulations. Because of the smaller density gradients of the TPG computations, a coarser resolution of 354×276 points could be used, above which very little overall change was observed. Maximum variation of some variables was less than 5 percent, while most of the resolved features look identical. Table 2 summarizes the flow conditions used in the simulations and the experiments.

The simulation model is implemented in parallel using MPI and employs a multi-domain framework. On an Intel Xeon cluster

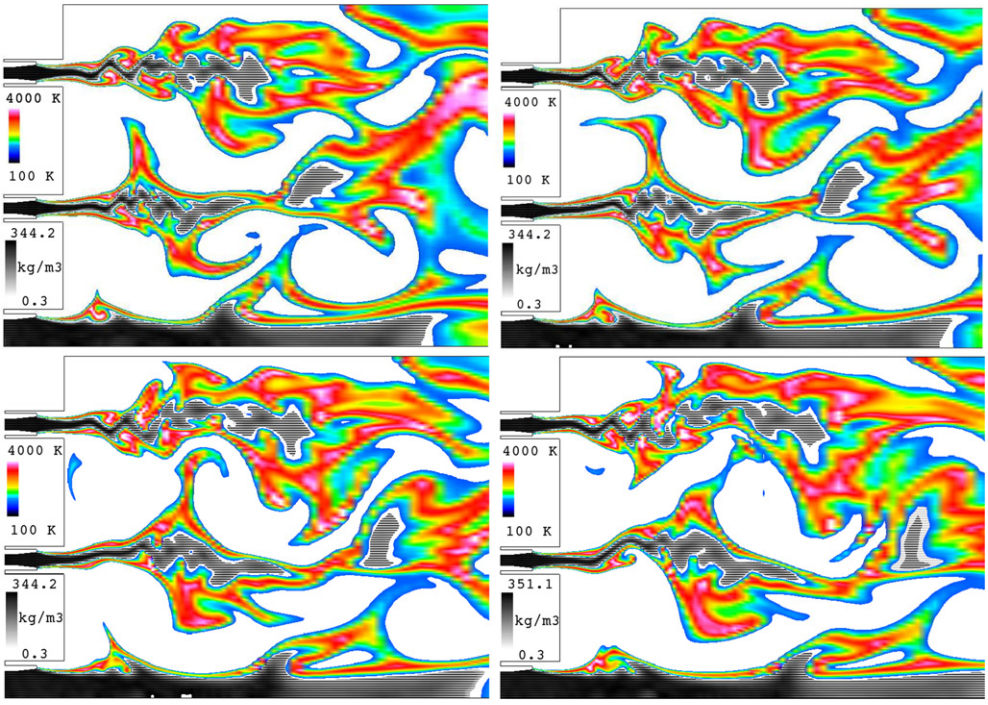

Fig. 1. Instantaneous density (in $\mathrm{kg\,m^{-3}}$, grey scale and stripes) and temperature (in K, color scale) fields at 4 consecutive instants (from left to right). Density smaller than 50 $\mathrm{kg\,m^{-3}}$ is not shown, effectively displaying the liquid core region. Temperature only higher than 1000 K is shown, effectively representing the combustion regions. (For interpretation of the references to color, the reader is referred to the web version of this article.)

with an Infiniband interconnect, a single flow-through time for the RG simulation requires approximately 1500 single-processor hours. The RG simulations are carried out for around 3 flow-through times after the initial transients to obtain properties for statistical analysis. The TPG simulations have been carried out much longer, typically 5–6 flow-through times after initial transients. In general, it has been determined that the mean properties are well converged after 3 flow-through times and the second-order moments converge within 6 flow-through times. Since, we are primarily interested in the mean properties (such as the mean heat flux) and in the transient features, the current simulation data is deemed acceptable.

4. Results and discussion

First, the focus is on general flow field observations such as the study of the instantaneous data, the analysis of time-averaged quantities and the flame structure. In general, features observed in the RG simulations are reported and referral to the TPG results is made when necessary. Finally, a more detailed comparison between TPG and RG simulations is performed, with a particular attention to the heat flux predictions. It is understood that the current study makes many assumptions in order to focus on the basic flow physics of a multiple-injector configuration with supercritical combustion. Given these assumptions, care was taken to obtain a robust solution independent of obvious parameters such as grid resolution or turbulent closure coefficients. As will be shown in this section, this means good quantitative results can be achieved on basic quantities such as temperature whereas mostly qualitative insight can be gained on complex phenomena such as the wall heat transfer. The conclusion will suggest directions on how to improve the accuracy of the current simulations.

4.1. Unsteady flow features

Fig. 1 shows a time sequence of the density (grey scale and stripes) and temperature (color scale) contours in the near field of the injectors for the RG simulation. The density contours show the state of the oxygen jet. Due to the supercritical injection condition, the incoming oxygen jet is not liquid but the density is close to the one of a liquid jet, as indicated by the dark areas in these figures. Further downstream, the jet seems to have a mixed liquid–gas behavior. Closer examination shows that each of the three injectors exhibits different flow and combustion patterns. The jet at the centerline cannot flap due to the centerline restriction. Thus, it looks very stable, and even though a shear mixing layer is present above it, the core stays mostly unperturbed for several diameters downstream. Limited combustion occurs in the thin mixing layer around the oxygen jet.

All the three injectors interact with each other. However, the behavior of the flow near each of them is different due to their relative locations. To understand this behavior and highlight the flow motion, Fig. 2 displays a time sequence of the vorticity contours superimposed with the velocity vector field. Comparison of both these figures shows that the middle injector interacts significantly with the other two through the shed vortices from the adjacent shear layers. Both the vorticity and velocity vector fields show that this shedding from the edges of each injector is periodic. Analysis of the time sequence of the vortex motion for the middle injector shows a frequency of 3.6 KHz (the other shedding frequency is similar). This corresponds to a Strouhal number $St = fD/U$ of 1.24 (using $D = 0.102$ m, the hydrogen step height, and $U = 300\ \mathrm{m\,s^{-1}}$, characteristic velocity of the hydrogen jet), which is in the jet preferred mode for a free jet. The low pressure region at the base of the steps between the three injectors offer a mechanism to create and maintain this vortex shedding process. Since the three step planes are of different height, the interactions are also different, with vortex sizes varying between 20 and 60 mm. This vortex shedding is related to the instability in the shear layers from each of the injectors. Overall, the interaction for the middle injector is the most dramatic since it is the only injector with true free-boundaries. As shown in Fig. 1, the resulting flapping instability leads to a pinch-off of the jet, with a pocket of dense, unburned oxygen being convected downstream. The outermost shear layer

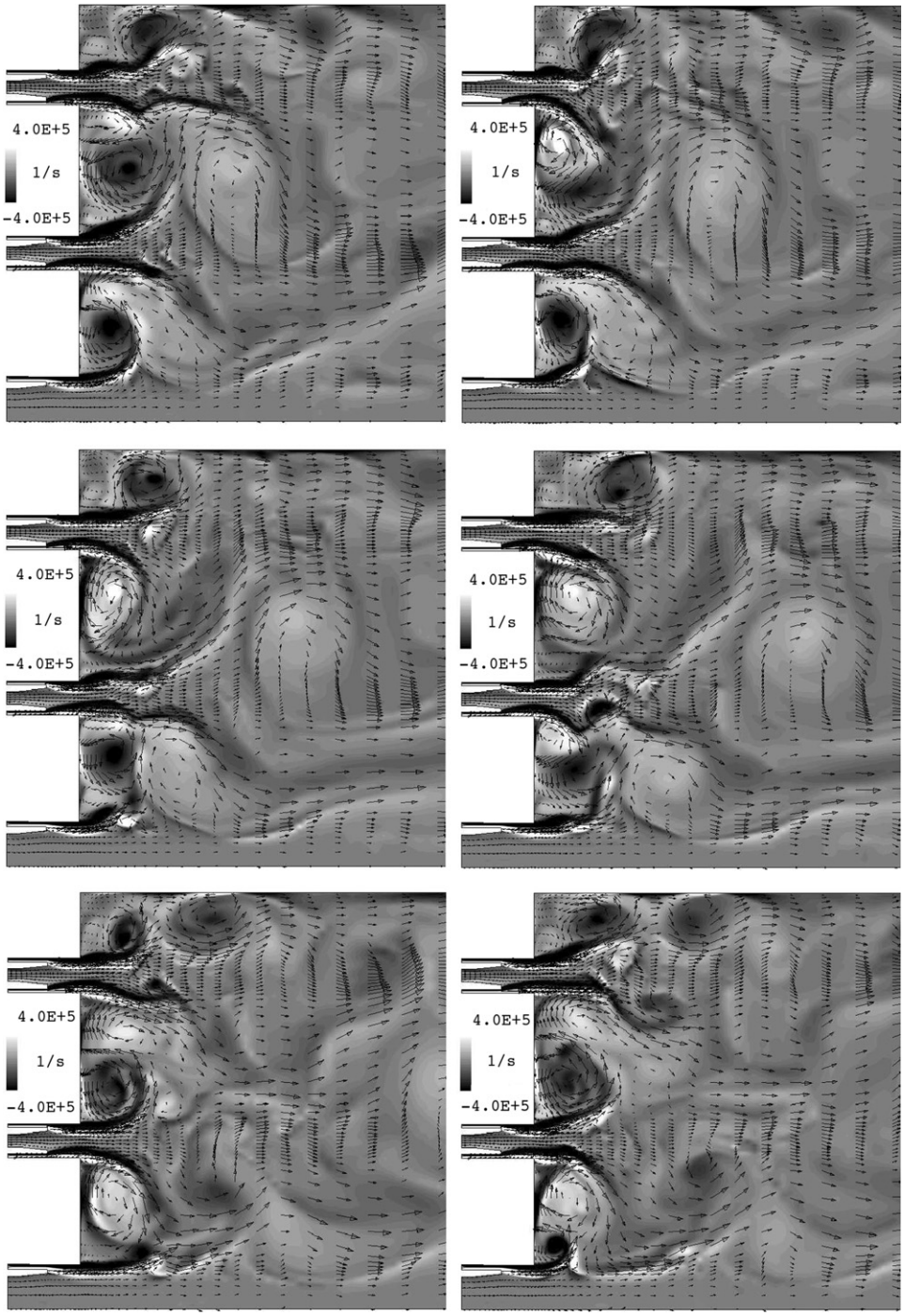

Fig. 2. Instantaneous vorticity (in 1/s) and velocity vector fields at 6 consecutive instants.

next to the combustor wall also shows some shedding, however the flapping is constrained by the wall. The impingement of this jet on the chamber wall will be shown to be critical for the transient heat flux.

The oxygen jet instability is also controlled by both thermodynamic (e.g., specific heat, heat release from combustion) and transport (e.g., viscosity, thermal conductivity, molecular diffusion) properties that must be computed accurately. All these properties display a wide range of values across the combustion chamber, with more than an order of magnitude difference for the transport properties between each reactant stream, or between the reactants and the burned products. Also, these variations extend further downstream than the variations of the compressibility parameter that are limited to the oxygen jets inner core, as seen on Fig. 2. This justifies our emphasis on getting an accurate estimate of these transport properties, since these large gradients play an important role in the overall flow behavior. This will be emphasized in the last part of this results section.

4.2. Analysis of time averaged quantities

The average pressure field (not shown here) is smooth without large fluctuations, and close within 1% to the nominal conditions in the bulk of the chamber. This has required some adjustment of the nominal throat size once it has been choked. The centerline pressure is within 5% of the nominal conditions even though some

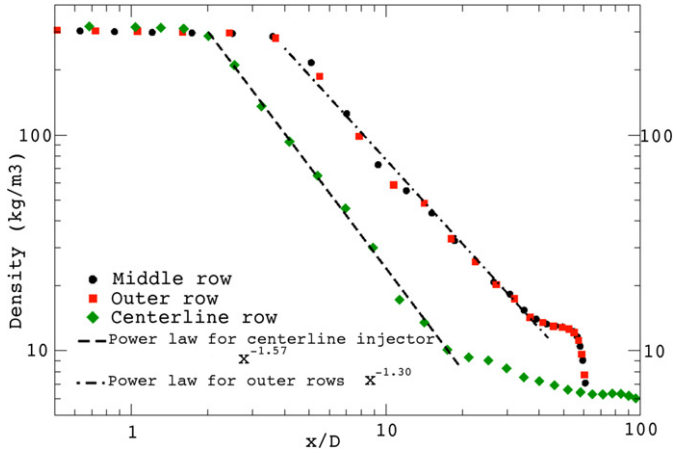

Fig. 3. Density decay downstream of the three injectors.

small oscillations occur, probably due to the centerline condition and the grid resolution there. However, these oscillations do not impact the results.

The difference between the centerline injector and the two other slots is qualitative when observing average fields such as density (not shown) or temperature (Fig. 4). It confirms the observations made on the instantaneous flow-field, and highlight the extent of the jet downstream, mainly due to the lack of radial motion along the centerline. For a more quantitative difference, Fig. 3 shows the density profiles against a non-dimensional coordinate x/D, where D is the diameter of the LOX inlet before the expansion of the coaxial injector. The origin is taken at the tip plane. It has to be noted that in this coordinate system, the injector plane does not have the same location for all injectors. The physical distance between the tip and the injector planes is 3.19 mm, which represents $1.24x/D$ for the outer rows, and $0.56x/D$ for the centerline injector. This explains the shift to the right of the outer profiles. Also, the lack of combustion along the centerline probably explains the slower decay further downstream for the centerline injector ($x/D > 20$). Taking into account these two features, we look at the dependence in x/D of the density profiles. In the region where they follow a power-law of the type:

$$\rho \propto \left(\frac{x}{D}\right)^n \tag{5}$$

the exponents are found to be close to the values given by Oschwald et al. [28], who report values below -1 for supercritical jets without combustion. This fact, and the relative small difference in slope between the centerline row and the outer rows, shows that the role of combustion on the initial mixing is limited. The early mixing between the two reactants is mostly influenced by the fluid mechanics and the transport properties. The flame anchoring mechanism in the near-field region is important for the complete combustion further downstream and will be more closely examined in the next section.

4.3. Flame structure

The location of the flame is of course very valuable information which has been the subject of much debate for this configuration. Very limited reliable measurements are available for supercritical combustion in a coaxial injector. Using new visualization techniques (planar laser light scattering, OH emission imaging, tomography) on sub-critical LOX/GH_2 flames, Herding et al. [13] claim that the flame is established in the outer boundary of the LOX jet, in a region of low velocity. However, Mayer et al. [18] reported

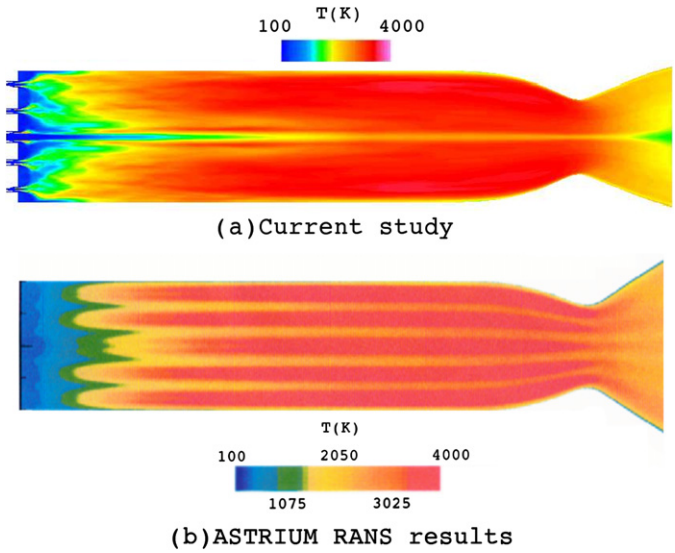

Fig. 4. Time-averaged temperature fields in K. Top figure shows the current study. Bottom figure shows RANS results from Preclik et al. [30].

that a pilot flame is anchored at the tip of the tube between the oxygen and the hydrogen under supercritical conditions, an observation confirmed by more recent studies [17,24].

The top of Fig. 4 shows the time-averaged temperature contours and confirms what was already apparent on Fig. 1. The flame is indeed attached to the sleeve that separates the two coaxial jets. This agrees with earlier observations where the flame was indeed observed in the recirculation region behind the tip. Whether the flame is in reality attached to the wall seems unlikely, but to prove it would require much finer resolution as well as an isothermal boundary condition at the tip. The mixing layer created in the wake of this wall is resolved in the current simulation with enough accuracy so that a continuous region of high temperature is always present. Additional analysis shows that this flame anchoring location is in a region of high strain rates ranging from 30 $\mathrm{m\,s^{-1}}$ to 300 $\mathrm{m\,s^{-1}}$. It is possible that such a high strain can cause flame extinction and lift-off, and could result in a lifted flame structure. However, flame extinction/re-ignition is a very complex process and detailed kinetics are needed to understand this process. In the current study, this high strain only results in a thin flame in the near-field of the injector.

Fig. 4 compares the temperature fields of the present study with previous numerical results [30] using RANS and a similar axisymmetric configuration. These simulations were performed assuming that both reactants were injected as sprays in the combustion chamber. Whereas the hydrogen was allowed to evaporate immediately, a supercritical LOX gasification model controlled the behavior of the oxygen spray. There are similarities and differences between these two fields. Both computations show temperature fields approaching their maximum values after approximately 0.08 m. Also the overall range of temperature is pretty similar in both cases. But the LES simulation shows even less combustion along the centerline than the RANS, probably because of the lack of extra radial dissipation in the LES. While the current effort produces similar results to RANS, LES simulations allow to take a closer look at the unsteady fluid mechanics that control the mixing (see Section 4.1) or the transient heat flux to the wall (see Section 4.4).

4.4. Comparison of TPG and RG models

Three cases are considered here. The classical TPG and RG models as well as the TPG model with the RG transport properties.

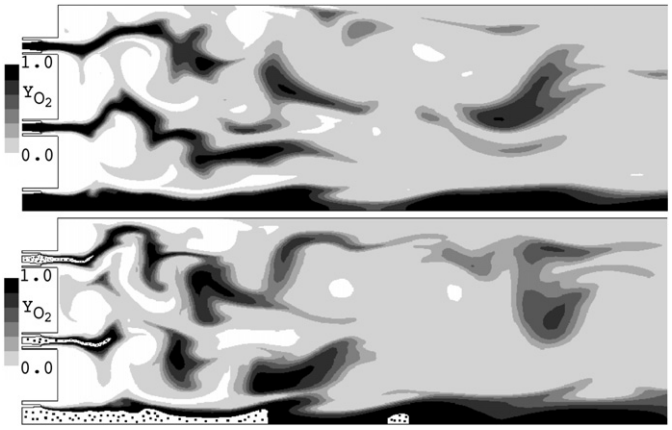

Fig. 5. Instantaneous oxygen mass fraction fields for the TPG run (top) and RG run (bottom). The figure for the RG also includes a dotted area where the compressibility is in the range 0.6–0.9, i.e. where the real gas effects are significant.

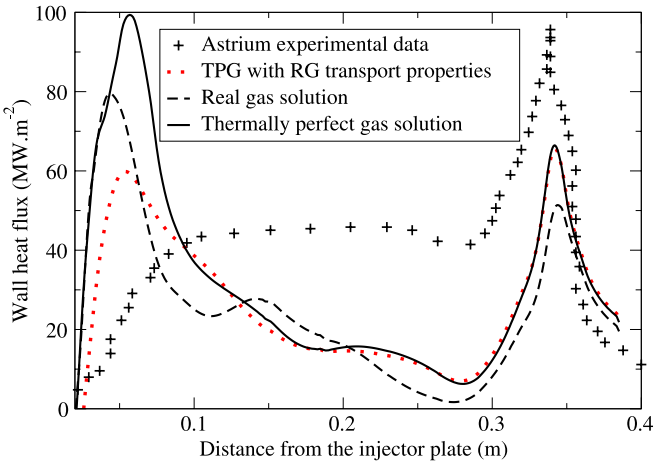

Fig. 6. Time-averaged heat flux through the combustion chamber wall for the RG case (dotted line) and the TPG case (full line).

This simulation combines Chung's methodology described previously and including high-pressure effects with the TPG framework. All simulations are started from the same initial real gas solution and run on the same grid of 601×382. They use the 2-step mechanism instead of the global mechanism. Since inflow boundary conditions enforce a constant mass flux, the inlet conditions for both runs are similar in terms of flow-rate, temperature and mass fractions. However, we expect the inlet densities and velocities to differ, especially for the supercritical oxygen jet for which the compressibility is significantly smaller than 1.

Only instantaneous results are discussed here, mainly because our interest is centered on the dynamics of the flow and on how the choice of the model can impact them. We have attempted to show characteristic figures that closely compare the flow features at (nearly) the same instant of flow development (identified here as the vortex shedding process from the injector tip).

On Fig. 5 which displays the instantaneous oxygen concentration for both cases, one can clearly see the different behavior that occurs under the TPG assumption. As stated before, the density of the oxygen jets is much lower for the TPG case (around 250 kg m^{-3}) than for the RG case (around 380 kg m^{-3}) and thus the inlet velocity for the oxygen is 50% higher in the TPG case. This has of course a direct impact on the dynamics of the jets since the velocity ratios have been changed. The breaking-up of the oxygen jets for the RG case seems to occur earlier than for the TPG case, leading to large, round pockets of unburned oxygen being convected downstream. The oxygen jets in the TPG case appear thinner and extend further in the flow without pinching. As a result, although both jets seem to flap in a similar fashion, the jet in the TPG case will impinge the wall further away from the injector plate. This will have a consequence on the wall heat flux. As expected, no change in the reported behavior of the centerline injector is observed between these 3 simulations.

Moreover, Fig. 5 for the RG case allows us to look at the extent of the real gas effects in the combustion chamber in terms of the compressibility Z. As mentioned before, the axisymmetric configuration and our assumptions to keep the velocity and momentum ratios close to the experimental values prevent us from having identical injectors. This explains why the real gas effects can be felt over a much larger region for the centerline injector. We even see that unburned pockets of oxygen, after having broken up from the jet, can experience significant departures from perfect gas behavior. This feature is not present in our simulation for the outer rows probably because their apparent diameter is smaller than what it should be in reality. For all jets, we can see that our RG model allows for a smooth transition between regions where the perfect gas model is not valid and where the compressibility is almost 1. Since the real gas model is very expensive in terms of computational resources, there is a need in the future to look at ways to bypass most of the RG computations when Z is sufficiently close to 1.

The average wall heat flux for both cases is shown in Fig. 6. First, the absolute level of heat flux, several tens of mega-watts per meter-square, is characteristic of those encountered in actual rocket engines. It is important that our simulations can represent such high values of heat transfer, which could represent a temperature gradient of approximately 1000 K over 20 microns, the characteristic distance of our first cell center to the wall. This plot seems to show that for both RG and TPG models, the sub-grid model is able to capture at least part of the physics occurring along the wall chamber. We can see that the peak value for the TPG model is higher and occurs further downstream compared to the RG simulation. This can be related to the jet dynamics described in the previous paragraphs, which showed that the jet flapping is different between the two cases. This flapping causes the heat transfer to the wall to be a very transient phenomenon.

Finally, the profile obtained for the simulation using the TPG model with the RG transport properties is also shown on Fig. 6. It underlines once again the influence of the transport properties on the jets dynamics with the difference between the pure TPG profile and the mixed TPG/RG profile. The oxygen jets for this mixed case have less inertia than for the RG case but are more viscous than the pure TPG case. As a result, the oxygen jets are much more constrained by the hydrogen annulus and the flapping is reduced. Thus, the smaller value of the initial maximum on the heat flux profile. Even though this local behavior is different, we are still injecting the same quantity of reactants under the same conditions as for the TPG case. Since far downstream from the injection, the RG formulation and RG transport properties recover to their TPG counterpart, it is logical that the profiles for the TPG simulation and the mixed simulation are the same. For the RG, the lower inlet velocity for the oxygen seems to lead to less turbulent sub-grid energy far downstream and thus to a lesser heat transfer in the later part of the chamber.

A region of particular interest is where the upper flapping jet impinges on the wall. Fig. 7 shows the instantaneous maximum heat flux and the location of this maximum. It can be seen that the unsteady impingement process generates small-scale turbulence and increases turbulent kinetic energy. However, this increase in turbulent kinetic energy cannot by itself explain the increase in heat flux. Indeed, the flame is also impinging on the wall and increases the temperature gradient. Combined, these two effects

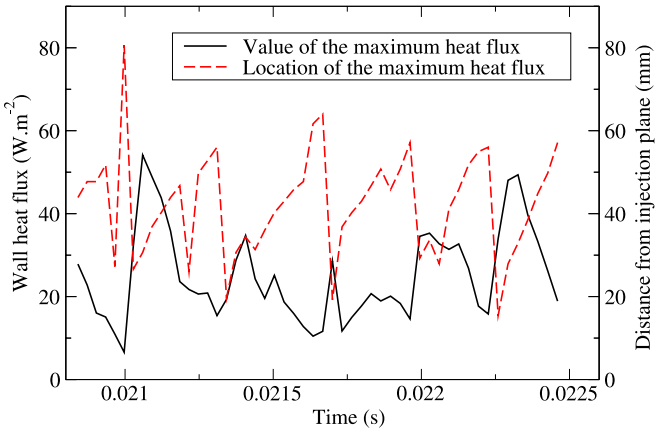

Fig. 7. Time history of maximum heat flux in the combustion chamber.

explain the unsteady peak that occurs at a frequency of approximately 3 kHz, which is close to the frequency observed in the vorticity spectra. This frequency is characteristic of the vortex shedding observed at the exit of the hydrogen jet. Analysis of the data shows that unsteady flapping of the jets will result in transient high heat flux on the combustor wall. However, this may not be observed on the outer walls that are being cooled (and where data is being obtained). Assuming the wall is made of stainless steel, we obtain a thermal thickness of approximately $6.5\sqrt{\kappa/\omega} \approx 2.4$ cm. Thus, if the wall is more than 2 cm thick, the cooling channel is not affected by the unsteady heat flux. In order to reach better agreement, we may have to reconsider our current assumption of fully isothermal wall and it may be necessary to solve the heat transport inside the chamber walls. This is an issue that will need additional effort in the future.

5. Conclusions

A new real gas/thermally perfect gas LES code using an axisymmetric approximation has been used to simulate unsteady combustion and dynamics in a representative LOX-GH_2 rocket engine consisting of three slot injectors that attempts to match the actual engine conditions. The purpose of this work was to prove the feasibility of such simulations and to assess their accuracy. The axisymmetric LES formulation allows such computations for a moderate cost. Different models for thermodynamic and transport properties can be used with this solver. However, limited experimental data are available in order to verify the validity of our different assumptions. Especially, no flow visualization of a multi-injector configuration is available, and only more global quantities have been measured as of today. Thus, the current LES simulations, with a reasonable qualitative agreement with the available experimental observations, give us an idea of the dynamics of a typical rocket combustion chamber.

Indeed the current LES simulations provide various point of views on what is occurring in a liquid rocket engine combustion chamber, where the combination of real gas effects and heat transfer effects makes its access very difficult and costly through experimentation. The examination of unsteady flow features through visualization or spectral analysis shows that vortex shedding and flame dynamics are intrinsically linked. In particular, the breakup of the oxygen jets by their surrounding shear layers controls the flame unsteadiness and thus the heat flux unsteadiness. The flame structure observed appears at least qualitatively correct with respect to what has been reported in the literature, especially the anchoring of the flame at the post LOX tip. Comparison between RG and TPG computations shows that real gas effects have an overall influence despite being limited to the core of the oxygen jets. Real gas transport properties have also a strong influence on the flow field and cannot be neglected while simulating such systems. Finally, although current simulations predict a higher heat flux in the near-injector region, new insight is gained on the unsteady nature of heat flux due to the transient impingement of the jet flame on the wall. Transient motion causes a wide variation in the heat flux on the gas side, even though, the high frequency associated with these transient events might prevent it from affecting the coolant side. Overall, many qualitative insights have been gained even if the quantitative accuracy of some quantities such as the wall heat flux can be questioned. The problem is that the wall heat flux is at the end of a long chain of physical processes and even if the predicted profile better match the experimental, it would be difficult to conclude that all the physics in the chamber were correctly captured. Thus, in parallel to the current effort, there is a need for more basic validation studies of high-pressure combustion in liquid rocket engines, under experimental conditions that hopefully allow easier access for flow visualization and detailed measurements. For future numerical studies, the inclusion of heat transport in the chamber walls and through radiation could reduce the uncertainty on the heat transfer but again, more care should first be applied to the coaxial supercritical combustion modeling. Full 3D simulations would remove the influence of the centerline and provide a more realistic modeling of coaxial jet dynamics. A hybrid upwind-central scheme [10] will allow a better control of the density gradients and a more accurate representation of the inflow boundary conditions. A more detailed mechanism, specifically tuned for H_2–O_2 systems under high pressure [21] might provide a more detailed flame structure and a more accurate flame holding mechanism. Finally, more refined sub-grid modeling for turbulence, mixing and combustion could provide even more accuracy and need to be validated under high-pressure conditions.

Acknowledgements

This work was supported by BMBF (German Ministry of Education and Research) in the framework of the ASTRA Program and a cooperation with EADS Astrium Ottobrunn (Astrium Space Transportation), Germany.

References

[1] A. Brink, C. Mueller, P. Kilpinen, M. Hupa, Possibilities and limitations of the eddy break-up model, Combustion and Flame 123 (2000) 275–279.
[2] S. Candel, M. Juniper, G. Singla, P. Scouflaire, C. Rolon, Structure and dynamics of cryogenic flames at supercritical pressure, Combustion Science and Technology 178 (2006) 161–192.
[3] J.V. Canino, J. Tsohas, V. Sankaran, S.D. Heister, Dynamic response of coaxial rocket injectors, in: 42nd AIAA/ASME/SAE/ASEE Joint Propulsion Conference and Exhibit, No. AIAA 2006-4707, Sacramento, CA, 2006.
[4] G.C. Cheng, R. Farmer, Real fluid modeling of multiphase flows in liquid rocket engine combustors, Journal of Propulsion and Power 22 (6) (2006) 1373–1381.
[5] T.H. Chung, M. Ajlan, L.L. Lee, K.E. Starling, Generalized multiparameter corresponding state correlation for polyatomic, polar fluid transport properties, Industrial and Chemical Engineering Research 27 (1988) 671–679.
[6] A. Congiunti, C. Bruno, E. Giacomazzi, Supercritical combustion properties, in: 41st Aerospace Sciences Meeting and Exhibit, No. AIAA 2003-478, Reno, NV, 2003.
[7] J.P. Drummond, M.Y. Hussaini, T.A. Zang, Spectral methods for modeling supersonic chemically reacting flowfields, AIAA Journal 24 (9) (1986) 1461–1467.
[8] G. Erlebacher, M.Y. Hussaini, C.G. Speziale, T.A. Zang, Toward the large-eddy simulation of compressible turbulent flows, Journal of Fluid Mechanics 238 (1992) 155–185.
[9] C. Fureby, On modeling of unsteady combustion utilizing continuum mechanical mixture theories and large eddy simulations, Ph.D. thesis, Lund Institute of Technology, Sweden, 1995.
[10] F. Génin, B. Fryxell, S. Menon, Hybrid large-eddy simulation of detonation in reactive mixtures, in: Proceedings of the 20th International Conference on Detonations, Explosions and Shock Waves, Montreal, Canada, 2005.

[11] M. Habiballah, M. Orain, F. Grisch, L. Vingert, P. Gicquel, Experimental studies of high-pressure cryogenic flames on the Marcotte facility, Combustion Science and Technology 178 (2006) 101–128.
[12] K.G. Harstad, J. Bellan, High-pressure binary mass-diffusion coefficients for combustion applications, Industrial and Engineering Chemistry Research 43 (2004) 645–654.
[13] G. Herding, R. Snyder, C. Rolon, S. Candel, Investigation of cryogenic propellant flames using computerized tomography of emission images, Journal Propulsion and Power 14 (2) (1998) 146–151.
[14] N. Ierardo, A. Congiunti, C. Bruno, Mixing and combustion in supercritical O_2/CH_4 liquid rocket injectors, in: 42nd Aerospace Sciences Meeting and Exhibit, No. AIAA 2004-1163, Reno, NV, 2004.
[15] H. Lou, R.S. Miller, On ternary species mixing and combustion in isotropic turbulence at high pressure, Physics of Fluids 16 (5) (2004) 1423–1438.
[16] M. Masquelet, Simulations of a sub-scale liquid rocket engine: Transient heat transfer in a real gas environment, Master's thesis, Georgia Institute of Technology, December 2006.
[17] W.O.H. Mayer, B. Ivancic, A. Schik, U. Hornung, Propellant atomization and ignition phenomena in liquid oxygen/gaseous hydrogen rocket combustors, Journal of Propulsion and Power 17 (4) (2001) 794–799.
[18] W.O.H. Mayer, H. Tamura, Propellant injection in a liquid oxygen/gaseous hydrogen rocket engine, Journal of Propulsion and Power 12 (1996) 1137–1147.
[19] R.S. Miller, J. Bellan, K.G. Harstad, Direct numerical simulations of supercritical fluid mixing layers applied to heptane-nitrogen, Journal of Fluid Mechanics 436 (2001) 1–39.
[20] NIST chemistry webbook, URL http://webbook.nist.gov/chemistry/fluid, 2005.
[21] M. O'Conaire, H.J. Curran, J.M. Simmie, W.J. Pitz, C.K. Westbrook, A comprehensive modeling study of hydrogen oxidation, International Journal of Chemical Kinetics 36 (2004) 603–622.
[22] J.C. Oefelein, Thermophysical characteristics of shear-coaxial LOX-H_2 flames at supercritical pressure, Proceedings of the Combustion Institute 30 (2005) 2929–2937.
[23] J.C. Oefelein, Mixing and combustion of cryogenic oxygen–hydrogen shear-coaxial jet flames at supercritical pressure, Combustion Science and Technology 178 (2006) 229–252.
[24] J.C. Oefelein, LES of supercritical LOX-H2 injection and combustion in a shear coaxial uni-element rocket, in: 41st Aerospace Sciences Meeting and Exhibit, No. AIAA 2003-0479, Reno, NV, 2003.
[25] N. Okong'o, J. Bellan, Consistent boundary conditions for multicomponent real gas mixtures based on characteristic waves, Journal of Computational Physics 176 (2002) 330–344.
[26] N. Okong'o, J. Bellan, Turbulence and fluid-front area production in binary-species, supercritical, transitional mixing layers, Physics of Fluids 16 (5) (2004) 1467–1492.
[27] N. Okong'o, J. Bellan, K.G. Harstad, Direct numerical simulations of O_2/H_2 temporal mixing layers under supercritical conditions, AIAA Journal 40 (5) (2002) 914–926.
[28] M. Oschwald, M.M. Micci, Spreading angle and centerline variation of density of supercritical nitrogen jets, Atomization and Sprays 11 (2002) 91–106.
[29] B.E. Poling, J.M. Prausnitz, J.P. O'Connell, The Properties of Gases and Liquids, fifth edition, McGraw-Hill, 2001.
[30] D. Preclik, D. Wiedmann, W. Oeschlein, J. Kretschmer, Cryogenic rocket calorimeter chamber experiments and heat transfer simulation, in: 34th AIAA/ASME/SAE/ASEE Joint Propulsion Conference and Exhibit, Cleveland, OH, AIAA 1998-3440.
[31] V. Sankaran, S. Menon, LES of scalar mixing in supersonic mixing layers, Proceedings of the Combustion Institute 30 (2005) 2835–2842.
[32] J.U. Schlüter, Influence of axisymmetric assumptions on large eddy simulations of a confined jet and a swirl flow, International Journal of Computational Fluid Dynamics 18 (3) (2004) 235–246.
[33] N. Tramecourt, S. Menon, J. Amaya, LES of supercritical combustion in a gas turbine engine, in: 40th AIAA/ASME/SAE/ASEE Joint Propulsion Conference and Exhibit, 2004.
[34] C. Tsonopoulos, J.L. Heidman, High-pressure vapor-liquid equilibria with cubic equations of state, Fluid Phase Equilibria 29 (1986) 391–414.
[35] P.K. Tucker, S. Menon, C.L. Merkle, J.C. Oefelein, V. Yang, An approach to improved credibility of CFD simulations for rocket injector design, in: 43rd AIAA/ASME/SAE/ASEE Joint Propulsion Conference and Exhibit, No. AIAA 2007-5572, Cincinnati, OH, 2007.
[36] V. Yang, J.C. Oefelein, Special triple issue on supercritical fluid transport and combustion, Combustion Science and Technology 178 (1–3) (2006) 1–621.
[37] N. Zong, V. Yang, Cryogenic fluid jets and mixing layers in transcritical and supercritical environments, Combustion Science and Technology 178 (2006) 193–227.
[38] N. Zong, V. Yang, Cryogenic fluid injection and mixing at supercritical condition, in: 41st Aerospace Sciences Meeting and Exhibit, Reno, NV, AIAA 2003-480.